

# Learning the Hierarchical Parts of Objects by Deep Non-Smooth Nonnegative Matrix Factorization

Jinshi Yu, Guoxu Zhou, Andrzej Cichocki *IEEE Fellow*, and Shengli Xie *IEEE Senior Member*

**Abstract**—Nonsmooth Nonnegative Matrix Factorization (*nsNMF*) is capable of producing more localized, less overlapped feature representations than other variants of NMF while keeping satisfactory fit to data. However, *nsNMF* as well as other existing NMF methods is incompetent to learn hierarchical features of complex data due to its shallow structure. To fill this gap, we propose a deep *nsNMF* method coined by the fact that it possesses a deeper architecture compared with standard *nsNMF*. The deep *nsNMF* not only gives parts-based features due to the nonnegativity constraints, but also creates higher-level, more abstract features by combing lower-level ones. The in-depth description of how deep architecture can help to efficiently discover abstract features in *dnsNMF* is presented. And we also show that the deep *nsNMF* has close relationship with the deep autoencoder, suggesting that the proposed model inherits the major advantages from both deep learning and NMF. Extensive experiments demonstrate the standout performance of the proposed method in clustering analysis.

**Index Terms**—nonnegative matrix factorization (NMF), *nsNMF*, Deep *nsNMF*, deep autoencoder, deep learning, face clustering, features learning, sparseness.

## I. INTRODUCTION

NONNEGATIVE matrix factorization (NMF) is a technique that represents a nonnegative data matrix  $\mathbf{X}$  as the product of two nonnegative matrices  $\mathbf{Z}$  and  $\mathbf{H}$ , i.e.,  $\mathbf{X} = \mathbf{ZH}$ , where  $\mathbf{Z}$  and  $\mathbf{H}$  are often called features and feature representation, respectively. Due to the nonnegativity constraints on  $\mathbf{Z}$  and  $\mathbf{H}$ , the representation is purely based on additive (without subtractive) combinations of entries. As a result, the columns of  $\mathbf{Z}$  can be viewed as basic building-blocks that compose  $\mathbf{X}$ , and the representation matrix  $\mathbf{H}$ , often very sparse, explains how to construct  $\mathbf{X}$  by superposing some of these building-blocks. For this reason, NMF has been a powerful tool in nonnegative data analysis and successfully applied in diverse areas including, but not limited to, environmetrics [1], microarray data analysis [2], [3], document clustering [4], [5], [6], face and objects recognition [7], [8], [9], [10], [11], [12], blind audio source separation [13], biomedical engineering [14], [15], [16], [2], polyphonic music transcription [17] and more.

Nevertheless, NMF often produces features with a very high degree of overlapping in practice, which contradicts our intuition of “parts-based” learning ability of NMF. In order to extract more localized, meaningful, and less overlapped features of the data, quite a number of NMF variants have been

proposed, including local nonnegative matrix factorization [18], nonnegative sparse coding [19], NMF with sparseness constraints [20], [21], just to mention a few. These NMF variants enforce sparseness of the features  $\mathbf{Z}$  or the feature representation  $\mathbf{H}$ , or both by using norm penalty. Unfortunately, using this method to improve the sparseness of either one of  $\mathbf{Z}$  and  $\mathbf{H}$  will eventually reduce the sparseness of the other one in order to keep reasonable fitting to the data matrix  $\mathbf{X}$ . And improving the sparseness of both will certainly increase the constructed error between  $\mathbf{X}$  and  $\mathbf{ZH}$ . To solve this dilemma, Pascual-Montano et al. proposed a non-smooth NMF (*nsNMF*) method by introducing a “smoothing” matrix  $\mathbf{S}$  into the NMF model [22], such that  $\mathbf{X} = \mathbf{ZSH}$ . The distinct advantage of *nsNMF* is that, by adjusting the smoothing factor  $\mathbf{S}$ , the sparsity of both the features matrix  $\mathbf{Z}$  and feature representation  $\mathbf{H}$  can be finely tuned while still keeping faithful fit of model to the original data. This feature makes *nsNMF* quite flexible and versatile in practical applications.

Usually, we perceive and understand a new object using concepts we have already known. Consequently, we recognize the world essentially using a hierarchical structure which presents many levels of understanding and abstraction of objects. In the lowest level, very detailed and concrete physical features are presented, whereas in the highest level, details are largely ignored and more abstract features are formed by combing lower level features. In other words, each level in this hierarchical structure creates a specific level of abstract perception. This has motivated the rapid development of deep learning, a powerful technique capable of extracting high-level abstract features of objects and has achieved great success in a wide range of machine learning tasks. As *nsNMF* always tends to learn low level features such as contours, corner, angles, and surface boundaries due to its shallow structure and sparseness enforcement, it is therefore meaningful to equip *nsNMF* with a deep architecture which allows it to extract parts-based and more abstract features of objects. To serve this purpose, we develop a new model called Deep *nsNMF* (*dnsNMF*) in this paper to perform deep decompositions in the sense that it contains multiple layers of *nsNMF*. The deep architecture of *dnsNMF* is expected to learn high level, more abstract features by combining lower level features, in order to model more complex data.

Note that Cichocki and Zdunek have proposed a simple multilayer NMF [23]–[25] to improve the performance of blind signal separation (BSS) about ten years ago. Although it is a good idea at that time, their works did not consider the solution to update the parameters globally and not the mechanism to keep the good fit of model to the original data. As the success

J. Yu, G. Zhou, and S. Xie are with the Faculty of Automation, Guangdong University of Technology, Guangzhou, 510006, China (E-mail: jinshi.yu@foxmail.com, gx.zhou@gdut.edu.cn, shlxie@gdut.edu.cn).

A. Cichochi is from RIKEN, Japan and SKOLTECH, Moscow, Russia

of deep learning, deep learning methods have been widely used in NMF field, such as N-NMF [26], deep semi-NMF [27] and SDNMF [28]. The key idea of [26] is performing the NMF/GNMF on the nonlinear dimension reduction of original data by resort to the deep learning method. Obviously, this method does not use the multilayer NMF and may lose some important information of raw data for the NMF task. In [27], a complete deep architecture was introduced to build a multi-layer semi-NMF and also consider many other nonlinear activation on factor matrices. Unfortunately deep semi-NMF ignores nonnegative property of the learned features and the sparse structure hidden in complex data. Recently, [28] adds the sparse constraints to factor matrix features or discriminative representation in the multilayer NMF and successfully explores the sparse structure of data by using the Nesterov's accelerated gradient descent algorithm. However, using this method to improve the sparseness of some factor matrices will reduce the sparseness of other ones in order to keep reasonable fitting to original data. Moreover, although these deep NMF methods achieve much improvement in complex data analysis, as we all know, they all lack of many important and necessary discussion, such as how a deep structure can help to efficiently discover abstract features in deep NMF and the relationship between deep NMF and deep learning. All these aspects have been considered in our paper. In particular, we build dnsNMF model by stacking one-layer *ns*NMF into multiple layers, as *ns*NMF has the advantage of simultaneously improving the sparseness of all factor matrices while keeping faithful fit of model to the original data. The reason that how a deep NMF can efficiently discover abstract features is described in III-A. And the description of relationship between deep NMF and deep learning is presented in Section 4.

The rest of the paper is organized as follows: In Section 2, a brief review of NMF and *ns*NMF is presented. In Section 3, the dnsNMF method is proposed and implementation details are provided. The relationship between dnsNMF and deep autoencoding is briefly explained in Section 4. How dnsNMF can be used to extract a hierarchy of different level of abstract features is visualized and experimental results on clustering are presented in Section 5. Finally, some concluding remarks and future works are given in Section 6.

## II. BACKGROUND

### A. Nonnegative Matrix Factorization (NMF)

We assume that the data matrix  $\mathbf{X} = [\mathbf{x}_1, \mathbf{x}_2, \dots, \mathbf{x}_n] \in \mathbb{R}_+^{p \times n}$  is a collection of  $n$  data samples as its columns, each with  $p$  features. Nonnegative matrix factorization (NMF) [29] finds a compact representation of  $\mathbf{X}$  such that

$$\mathbf{X} \approx \mathbf{Z}\mathbf{H}, \mathbf{Z} \geq \mathbf{0}, \mathbf{H} \geq \mathbf{0}, \quad (1)$$

where  $\mathbf{Z} \in \mathbb{R}_+^{p \times r}$  is the matrix of basis vectors, and  $\mathbf{H} \in \mathbb{R}_+^{r \times n}$  the encoding vectors or projections,  $r \leq \min\{p, n\}$ , all matrices  $\mathbf{X}$ ,  $\mathbf{Z}$ ,  $\mathbf{H}$  are nonnegative.

In practice, NMF can be implemented by minimizing the distance between the original data  $\mathbf{X}$  and its low-rank

representation  $\mathbf{Z}\mathbf{H}$ . One of the most widely used distance measurements is the Euclidean distance, defined as:

$$E(\mathbf{Z}, \mathbf{H}) = \frac{1}{2} \sum_{i=1}^p \sum_{j=1}^n (\mathbf{x}_{ij} - (\mathbf{Z}\mathbf{H})_{ij})^2 = \frac{1}{2} \|\mathbf{X} - \mathbf{Z}\mathbf{H}\|_F^2. \quad (2)$$

Lee and Seung derived the following multiplicative update rules [29] to minimize the cost function (2):

$$\mathbf{H} \leftarrow \mathbf{H} \circledast \frac{\mathbf{Z}^T \mathbf{X}}{\mathbf{Z}^T \mathbf{Z} \mathbf{H}}, \quad (3)$$

$$\mathbf{Z} \leftarrow \mathbf{Z} \circledast \frac{\mathbf{X} \mathbf{H}^T}{\mathbf{Z} \mathbf{H} \mathbf{H}^T}, \quad (4)$$

where  $\circledast$  is the Hadamard product (i.e., element-wise product) of matrices. The multiplicative update rules have been widely adopted in NMF as they are easy to implement and also exhibit satisfactory trade-off between the accuracy and the speed of convergence. The NMF algorithm based on the multiplicative update rules (3) and (4), which is denoted as MU-NMF, can be summarized as follows:

- 1) Initialize  $\mathbf{Z}$  and  $\mathbf{H}$  such that both are element-wisely positive.
- 2) Update  $\mathbf{H}$  using (3) with fixed  $\mathbf{Z}$ .
- 3) Update  $\mathbf{Z}$  using (4) with fixed  $\mathbf{H}$ .

Repeat the above steps 2) and 3) until convergence. More details about MU-NMF can be found in [29].

### B. The *ns*NMF Method

Arguing that standard NMF often fails to give really parts-based representation if without additional regularizations, Pascual-Marqui et al. proposed the following non-smooth NMF (*ns*NMF) model [22]

$$\mathbf{X} = \mathbf{Z}\mathbf{S}\mathbf{H}, \mathbf{Z} \geq \mathbf{0}, \mathbf{H} \geq \mathbf{0}, \quad (5)$$

where matrices  $\mathbf{X}$ ,  $\mathbf{Z}$  and  $\mathbf{H}$  are the same as those in NMF. The positive symmetric matrix  $\mathbf{S} \in \mathbb{R}_+^{r \times r}$  is a ‘‘smoothing’’ matrix defined as:

$$\mathbf{S} = (1 - \theta) \mathbf{I} + \frac{\theta}{r} \mathbf{1}\mathbf{1}^T \quad (6)$$

where  $\mathbf{I}$  is the identity matrix,  $\mathbf{1}$  is a vector of ones, and the parameter  $\theta$  satisfies  $0 \leq \theta \leq 1$ .

The degree of smoothness of  $\mathbf{S}$  is controlled by the parameter  $\theta$ . As  $\theta \rightarrow 1$ , the matrix  $\mathbf{S}$  becomes more smooth as it tends to be a constant matrix with all elements almost equal. Note that a more smooth matrix  $\mathbf{S}$  will enforce stronger sparseness in both  $\mathbf{Z}$  and  $\mathbf{H}$  in order to maintain faithful fit of the model to the data. In other words, the parameter  $\theta$  controls the sparseness of both  $\mathbf{Z}$  and  $\mathbf{H}$ .

## III. DEEP *ns*NMF FOR HIERARCHY FEATURE EXTRACTION

### A. The Model

The goal of *ns*NMF is to find localized and less overlapped features of data by using a relatively large value of  $\theta$ . As a result, *ns*NMF always tends to learn low level features such as contours, corners, angles, and surface boundaries. This is just

the motivation behind the  $ns$ NMF method. On the contrary, when  $\theta = 0$ ,  $ns$ NMF boils down to ordinary NMF and may give non-sparse, largely overlapped features. In many practical applications, the data we wish to analyze is rather complex and is often produced by a mix model with many variables and factors. In order to better understand such complex data, it becomes compelling to disentangle the variables and extract low and high level features simultaneously. To fulfill this purpose, we propose a modified  $ns$ NMF with deep architecture (called  $dns$ NMF). In  $dns$ NMF, the data is represented using a multilayer structure:

$$\mathbf{X} = \mathbf{Z}_1 \mathbf{S}_1 \mathbf{Z}_2 \mathbf{S}_2 \cdots \mathbf{Z}_m \mathbf{S}_m \mathbf{H}_m, \quad (7)$$

which generates a total of  $m$  layers of features given by

$$\begin{aligned} \mathbf{W}_1 &= \mathbf{Z}_1, \\ \mathbf{W}_2 &= \mathbf{Z}_1 \mathbf{S}_1 \mathbf{Z}_2, \\ &\vdots \\ \mathbf{W}_m &= \mathbf{Z}_1 \mathbf{S}_1 \mathbf{Z}_2 \mathbf{S}_2 \cdots \mathbf{Z}_m, \end{aligned} \quad (8)$$

each of which is expected to develop a different level of abstraction. The  $m$  layers of features reflect the hierarchy and structural information contained in  $\mathbf{X}$ . In the meanwhile,  $\mathbf{W}_1$  is the lowest level features, denoting largely fragmental and very concrete features of objects, and  $\mathbf{W}_m$  is in the highest level and denotes more meaningful and abstract features. Moreover, from (8) we have

$$\mathbf{W}_i = \mathbf{W}_{i-1} \mathbf{S}_i \mathbf{Z}_i, \quad i = 2, 3, \dots, m, \quad (9)$$

implying that higher-level features are additive combinations of lower-level features. Particularly, (7) can be viewed as a cascade of  $ns$ NMF (See Fig.1). Taking the power of both  $ns$ NMF and deep learning into account,  $dns$ NMF is expected to be able to: (1) Automatically learn hierarchical features, where the higher level features are the combination of lower level features; (2) Achieve a high degree of sparseness in both the feature factors and feature representation, which largely retains the parts-based learning ability of  $ns$ NMF. To understand the intuition of  $dns$ NMF, features extracted by a 3-layer  $dns$ NMF by using the CBCL database are shown in Fig.3. It can be seen from Fig.3(b) that, features in the first layer mostly are pixels and outlines. In the second layer, connected edges and contours of facial parts (nose, lips, eyebrow) appear, as shown in Fig.3(c). In the third layer, some entire facial parts like nose, lips, and eyebrow are visibly presented, see Fig.3(d).

### B. Nesterov-type Optimization for $dns$ NMF

The Deep  $ns$ NMF algorithm consists of two key stages: pre-training and fine-tuning. In the pre-training stage, the original data matrix  $\mathbf{X}$  is decomposed using the  $ns$ NMF model, i.e.,  $\mathbf{X} \approx \mathbf{Z}_1 \mathbf{S}_1 \mathbf{H}_1$ , where  $\mathbf{Z}_1 \in \mathfrak{R}_+^{p \times r_1}$ ,  $\mathbf{S}_1 \in \mathfrak{R}_+^{r_1 \times r_1}$  and  $\mathbf{H}_1 \in \mathfrak{R}_+^{r_1 \times n}$ . Then, the representation matrix is again factorized using  $ns$ NMF such that  $\mathbf{H}_1 = \mathbf{Z}_2 \mathbf{S}_2 \mathbf{H}_2$ , where  $\mathbf{Z}_2 \in \mathfrak{R}_+^{r_1 \times r_2}$ ,  $\mathbf{S}_2 \in \mathfrak{R}_+^{r_2 \times r_2}$  and  $\mathbf{H}_2 \in \mathfrak{R}_+^{r_2 \times n}$ . This procedure will continue till a desired depth has been reached.

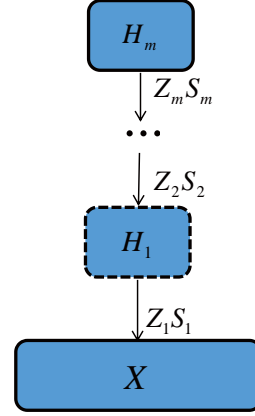


Fig. 1: Deep  $ns$ NMF learns a hierarchy of different level features that aid in uncovering the final high level feature representation of the data.

In the fine-tuning stage, the factor matrices in all layers will be fine-tuned using a global-like minimization. In detail, the following optimization problem will be solved:

$$\begin{aligned} E_{Deep}(\mathbf{Z}_1, \mathbf{Z}_2, \dots, \mathbf{Z}_m, \mathbf{H}_m) \\ = \frac{1}{2} \|\mathbf{X} - \mathbf{Z}_1 \mathbf{S}_1 \mathbf{Z}_2 \mathbf{S}_2 \cdots \mathbf{Z}_m \mathbf{S}_m \mathbf{H}_m\|_F^2. \end{aligned} \quad (10)$$

Apparently, the problem is highly non-convex and it is unrealistic to expect to find global solutions. Taking into account that the cost function is convex with respect to each single factor matrix, a common practice to solve this problem is applying the block coordinate descend method, i.e., minimizing the cost function with respect to only one factor matrix each time, while remaining the others fixed. Note that every factor matrix must be updated at least once after a certain number of iterations, which is often referred to as a sweep. Below we discuss how to update each factor matrix.

- *Update  $\mathbf{Z}_1$  and  $\mathbf{H}_m$ .* This is the simplest case as these two cases actually have been extensively studied in nonnegative matrix/tensor factorization. When all factor matrices but  $\mathbf{H}_m$  are fixed, problem (10) is equivalent to the following optimization problem:

$$\min_{\mathbf{H}_m \geq 0} E_{Deep}(\mathbf{H}_m) = \frac{1}{2} \|\mathbf{X} - \mathbf{A} \mathbf{H}_m\|_F^2. \quad (11)$$

where

$$\mathbf{A} = \mathbf{Z}_1 \mathbf{S}_1 \mathbf{Z}_2 \mathbf{S}_2 \cdots \mathbf{Z}_m \mathbf{S}_m. \quad (12)$$

Problem (11) is a standard nonnegative least squares problem, and any state-of-the-art methods in [30]–[32] can be applied. As all these methods are essentially the first-order methods, we are particularly interested in the accelerated proximal gradient (APG) method, which is often viewed as the optimal first-order method. While the details of APG based NMF/NTF can be found in [31], [32], we briefly introduce the APG method here to make paper self-contained.

*Lemma 1 ([31], [32]):* The gradient of  $E_{deep}(\mathbf{H}_m)$ , i.e.,

$$\nabla_{\mathbf{H}_m} E_{deep}(\mathbf{H}_m) = \mathbf{A}^T \mathbf{A} \mathbf{H}_m - \mathbf{A}^T \mathbf{X}, \quad (13)$$

---

**Algorithm 1** The APG Algorithm for  $\min_{\mathbf{H}_m} E_{deep}(\mathbf{H}_m)$ .

---

**Require:**  $\mathbf{X}, \mathbf{A}$  given in (12)

- 1: Initialize  $\mathbf{H}_m^k, \mathbf{Y}^k = \mathbf{H}_m^k, \alpha_0 = 1, k = 0. L = \|\mathbf{A}^T \mathbf{A}\|_2$ .
  - 2: **while** not coverage **do**
  - 3:  $\mathbf{H}_m^{k+1} \leftarrow \mathcal{P}_+ \left( \mathbf{Y}^k - \frac{1}{L} \nabla_{\mathbf{H}_m} E_{deep} |_{\mathbf{H}_m = \mathbf{Y}^k} \right)$ .
  - 4:  $\alpha_{k+1} \leftarrow \frac{1 + \sqrt{4\alpha_k^2 + 1}}{2}$ .
  - 5:  $\mathbf{Y}^{k+1} \leftarrow \mathbf{H}_m^{k+1} + \frac{\alpha_k - 1}{\alpha_{k+1}} (\mathbf{H}_m^{k+1} - \mathbf{H}_m^k)$ .
  - 6:  $k \leftarrow k + 1$ .
  - 7: **end while**
  - 8: **return**  $\mathbf{H}_m = \mathbf{H}_m^k$ .
- 

is Lipschitz continuous and  $L = \|\mathbf{A}^T \mathbf{A}\|_2$  is a Lipschitz constant.

We briefly explain the core idea of the APG method below. For notational simplicity we temporarily define

$$g(\mathbf{H}_m) \doteq E_{deep}(\mathbf{H}_m). \quad (14)$$

Then, the Lipschitz constant  $L$  ensures that,  $\forall \mathbf{H}, \tilde{\mathbf{H}}$ ,

$$\left\| g'(\mathbf{H}) - g'(\tilde{\mathbf{H}}) \right\|_F \leq L \left\| \mathbf{H} - \tilde{\mathbf{H}} \right\|_F, \quad (15)$$

thereby leading to [33, Appendix A.24]

$$\begin{aligned} g(\mathbf{H}) &\leq \phi(\mathbf{H}) \\ &\doteq g(\tilde{\mathbf{H}}) + \langle g'(\tilde{\mathbf{H}}), \mathbf{H} - \tilde{\mathbf{H}} \rangle + \frac{L}{2} \left\| \tilde{\mathbf{H}} - \mathbf{H} \right\|_F^2. \end{aligned} \quad (16)$$

The APG method minimizes the upper bound  $\phi(\mathbf{H})$  instead of  $g(\mathbf{H})$  directly. Note that  $\phi(\mathbf{H})$  is convex w.r.t.  $\mathbf{H}$  and the global optimum is  $\mathcal{P}_+ \left( \tilde{\mathbf{H}} - \frac{1}{L} g'(\tilde{\mathbf{H}}) \right)$ , where the operator  $\mathcal{P}_+(\cdot)$  sets all negative entries to be zeros. Hence, we optimize  $g(\mathbf{H}_m)$  by updating  $\mathbf{H}_m$  iteratively using

$$\mathbf{H}_m \leftarrow \mathcal{P}_+ \left( \tilde{\mathbf{H}} - \frac{1}{L} g'(\tilde{\mathbf{H}}) \right). \quad (17)$$

Let  $\mathbf{H}_m^k$  be the value of  $\mathbf{H}_m$  after  $k$  iterations. It can be verified that

- 1) if  $\tilde{\mathbf{H}} = \mathbf{H}_m^k$ , (17) leads to a projected gradient method with the convergence rate no worse than  $\mathcal{O}(1/k)$ .
- 2) if  $\tilde{\mathbf{H}} = \mathbf{H}_m^k + \frac{\alpha_k - 1}{\alpha_k} (\mathbf{H}_m^k - \mathbf{H}_m^{k-1})$ , where the sequence  $\{\alpha_k\}$  satisfies  $\alpha_k^2 - \alpha_k \leq \alpha_{k-1}^2$ , (17) leads to a very fast convergence rate of  $\mathcal{O}(1/k^2)$ . See [32], [34] for detailed discussion.

In summary, problem (11) can be efficiently solved by using the APG method, see Algorithm 1 for the pseudo-code.

Similarly, by fixing all factors but  $\mathbf{Z}_1$ , problem (10) is equivalent to

$$\mathbf{Z}_1 = \arg \min_{\mathbf{Z}_1} E_{Deep}(\mathbf{Z}_1) = \frac{1}{2} \left\| \mathbf{X}^T - \mathbf{B}^T \mathbf{Z}_1^T \right\|_F^2, \quad (18)$$

where  $\mathbf{B} = \mathbf{S}_1 \mathbf{Z}_2 \mathbf{S}_2 \cdots \mathbf{Z}_m \mathbf{S}_m \mathbf{H}_m$ , and again it can be solved by applying Algorithm 1 similarly.

• *Update  $\mathbf{Z}_i$  for  $i = 2, 3, \dots$ .* By fixing all factors but  $\mathbf{Z}_i$ ,  $i > 1$ , we obtain

$$\mathbf{Z}_i = \arg \min_{\mathbf{Z}_i} E_{Deep}(\mathbf{Z}_i) = \frac{1}{2} \left\| \mathbf{X} - \mathbf{A}_i \mathbf{Z}_i \mathbf{B}_i \right\|_F^2, \quad (19)$$

---

**Algorithm 2** The dnsNMF algorithm.

---

**Require:**  $\mathbf{X} \in \mathbb{R}^{p \times n}$  and the layer sizes  $[r_1, r_2, \dots, r_m]$

**Output:** Feature factors  $\mathbf{Z}_i$  and feature presentation  $\mathbf{H}_m$  such that  $\mathbf{X} \approx \mathbf{Z}_1 \mathbf{S}_1 \mathbf{Z}_2 \mathbf{S}_2 \cdots \mathbf{Z}_m \mathbf{S}_m \mathbf{H}_m$ , where  $\mathbf{Z}_i \in \mathbb{R}_+^{r_{i-1} \times r_i}$ ,  $1 \leq i \leq m$ ,  $r_0 = p$ , and  $\mathbf{H}_m \in \mathbb{R}_+^{r_m \times n}$ .

1: Initialize for  $t = 1$ :

$$(\mathbf{Z}_1^t, \mathbf{S}_1^t, \mathbf{H}_1^t) \leftarrow nsNMF(\mathbf{X});$$

$$(\mathbf{Z}_i^t, \mathbf{S}_i^t, \mathbf{H}_i^t) \leftarrow nsNMF(\mathbf{H}_{i-1}^t), \text{ for } i = 2, 3, \dots, m.$$

2: **repeat**

$$3: \mathbf{B} = \mathbf{S}_1 \mathbf{Z}_2 \mathbf{S}_2 \cdots \mathbf{Z}_m \mathbf{S}_m \mathbf{H}_m^t.$$

$$4: \mathbf{Z}_1^{t+1} \leftarrow \arg \min_{\mathbf{Z}_1} \frac{1}{2} \left\| \mathbf{X}^T - \mathbf{B}^T \mathbf{Z}_1^T \right\|_F^2 \text{ by using, say, the APG method.}$$

5: **for**  $i = 2$  **to**  $m$  **do**

$$6: \mathbf{A}_i = \mathbf{Z}_1^{t+1} \mathbf{S}_1 \cdots \mathbf{Z}_{i-1}^{t+1} \mathbf{S}_{i-1}.$$

$$7: \mathbf{B}_i = \mathbf{S}_i \mathbf{Z}_{i+1}^t \cdots \mathbf{S}_m \mathbf{H}_m^t.$$

$$8: \mathbf{Z}_i^{t+1} \leftarrow \arg \min_{\mathbf{Z}_i} \frac{1}{2} \left\| \mathbf{X} - \mathbf{A}_i \mathbf{Z}_i \mathbf{B}_i \right\|_F^2.$$

9: **end for**

$$10: \mathbf{A} = \mathbf{Z}_1^{t+1} \mathbf{S}_1 \mathbf{Z}_2^{t+1} \mathbf{S}_2 \cdots \mathbf{Z}_m^{t+1} \mathbf{S}_m.$$

$$11: \mathbf{H}_m^{t+1} \leftarrow \arg \min_{\mathbf{H}_m} \frac{1}{2} \left\| \mathbf{X} - \mathbf{A} \mathbf{H}_m \right\|_F^2.$$

$$12: t \leftarrow t + 1.$$

13: **until** A stopping criterion is met

---

where

$$\mathbf{A}_i = \mathbf{Z}_1 \mathbf{S}_1 \cdots \mathbf{Z}_{i-1} \mathbf{S}_{i-1},$$

$$\mathbf{B}_i = \mathbf{S}_i \mathbf{Z}_{i+1} \cdots \mathbf{S}_m \mathbf{H}_m, \quad i > 1.$$

In order to optimize  $\mathbf{Z}_i$  using the APG method, we need to show that the gradient  $\nabla_{\mathbf{Z}_i} E_{deep}(\mathbf{Z}_i)$  is also Lipschitz continuous. Note that the cost function  $E_{Deep}(\mathbf{Z}_i)$  can be rewritten in a vector form as

$$E_{Deep}(\mathbf{Z}_i) = \left\| \text{vec}(\mathbf{X}) - (\mathbf{B}_i^T \otimes \mathbf{A}_i) \text{vec}(\mathbf{Z}_i) \right\|_F^2, \quad (20)$$

where  $\text{vec}(\mathbf{Z}_i)$  is the vectorization operator of the matrix  $\mathbf{Z}_i$ , and  $\otimes$  is the Kronecker product of matrices. As such, (20) possesses exactly the same form as (11) and (18), and can be minimized similarly. By following the analysis in [31], [35], we have the following proposition:

*Proposition 1:* The gradient of  $E_{Deep}(\mathbf{Z}_i)$ , i.e.,

$$\nabla_{\mathbf{Z}_i} E_{deep}(\mathbf{Z}_i) = \mathbf{A}_i^T \mathbf{A}_i \mathbf{Z}_i \mathbf{B}_i \mathbf{B}_i^T - \mathbf{A}_i^T \mathbf{X} \mathbf{B}_i^T, \quad (21)$$

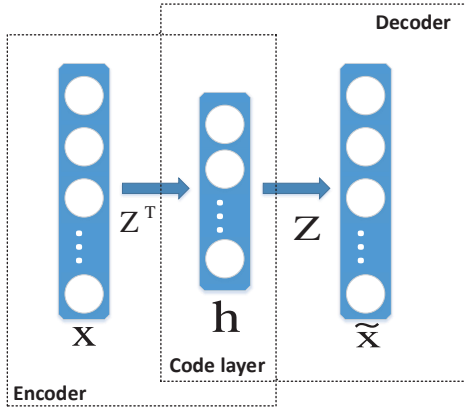
is Lipschitz continuous and  $L_i = \|\mathbf{A}_i^T \mathbf{A}_i\|_2 \|\mathbf{B}_i \mathbf{B}_i^T\|_2$  is a Lipschitz constant.

The proof is rather straightforward and can be found in Appendix A. Due to (21) and Proposition 1, the matrices  $\mathbf{Z}_i$  can be updated using the APG method efficiently.

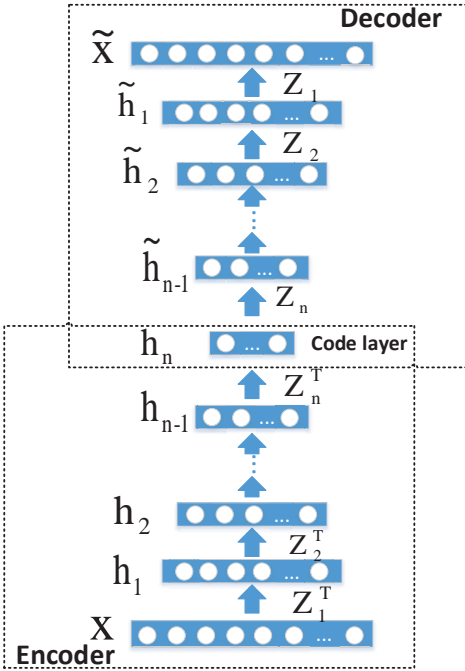
We summarize the dnsNMF algorithm in Algorithm 2.

#### IV. RELATIONSHIP BETWEEN DNSNMF WITH AUTOENCODER

It is well known that autoencoders [36] may be thought of as a special case of feedforward networks, which are able to extract representation of data with significantly reduced dimensionality. The structure of an autoencoder is shown in Fig.2(a). Typically, an autoencoder consists of two parts:



(a) Autoencoder



(b) Deep Autoencoder

Fig. 2: Illustration of autoencoder and deep autoencoder

an encoder function  $\mathbf{h} = f(\mathbf{x})$  that transforms the high dimensional data into a low-dimensional code, and a decoder that produces the reconstruction  $\tilde{\mathbf{x}} = g(\mathbf{h})$  that approximates the original data from the output of the encoder. The two parts are generally pre-trained together by minimizing the discrepancy between the original data and its reconstruction [37].

To create a deep autoencoder, multiple layers of encoder and decoder will be stacked in order, as illustrated in Fig.2(b). In the encoding stage, the output of each layer will be the input of its neighbored upper layer, and the dimensionality of outputs will be smaller and smaller, implying a more abstract and more compact representation of the original data. In the decoding stage, the encoding layers are “unrolled” to reconstruct the original data.

It can be seen that dnsNMF has the same structure as autoencoder. In the encoding stage, data are compressed with

both nonnegativity and sparsity constrained feature representations and weights, which preserves the learning parts ability of NMF. Due to the nonnegativity nature of outputs of *ns*NMF, we may assume that the rectified linear units (ReLU) are applied in the sense that  $g(\mathbf{Z}_l \mathbf{S}_l \mathbf{h}_l) = \mathbf{Z}_l \mathbf{S}_l \mathbf{h}_l$ , where  $g(x) = \max(0, x)$  is the rectified linear activation function. As such, dnsNMF can be represented as

$$\begin{aligned} \tilde{\mathbf{x}} &= g(\mathbf{Z}_1 \mathbf{S}_1 \tilde{\mathbf{h}}_1), \\ \tilde{\mathbf{h}}_1 &= g(\mathbf{Z}_2 \mathbf{S}_2 \tilde{\mathbf{h}}_2), \\ &\vdots \\ \tilde{\mathbf{h}}_{m-1} &= g(\mathbf{Z}_m \mathbf{S}_m \mathbf{h}_m). \end{aligned} \quad (22)$$

or equivalently in a compact form,

$$\mathbf{x} \approx \tilde{\mathbf{x}} = g(\mathbf{Z}_1 \mathbf{S}_1 g(\mathbf{Z}_2 \cdots g(\mathbf{Z}_m \mathbf{S}_m \mathbf{h}_m))), \quad (23)$$

implying that dnsNMF has the same structure as autoencoder.

Certainly, it also should be note that there are some differences between dnsNMF and deep autoencoder. dnsNMF is a unsupervised learning method which does not need data labels, but deep autoencoder is a semi-supervised learning method which uses unsupervised learning method to pre-train network and utilizes the supervised learning method to fine-tune it. dnsNMF, as an unsupervised learning method, can be applied to explore the unknown hierarchical features hidden in data while deep autoencoder are often be used to extract the features which are related to the data labels. From this point, they play different roles in data analysis and it is not significant to tell which is the better method.

## V. SIMULATIONS AND EXPERIMENTS

In this section, the proposed dnsNMF method was compared with related state-of-the-art methods by performing clustering analysis on three human face data sets, i.e. the ORL data set, the Jaffe data set, and the Yale data set. We also demonstrated abilities of the dnsNMF to extract sparse hierarchical features of data by using the CBCL data set.

### A. Data Sets

Four data sets were used in our experiments:

- AT&T ORL<sup>1</sup>: The AT&T ORL database consists of 10 different images for each of 40 distinct subjects, thus 400 images in total. The images were taken at different time with varying lighting, facial expressions (open/closed eyes, smiling/not smiling), and facial details (glasses/no glasses). All the images were taken against a dark homogeneous background with the subjects in an upright, frontal position.
- JAFFE<sup>2</sup>: The database contains 213 images of 7 facial expressions (6 basic facial expressions + 1 neutral) posed by 10 Japanese female models. Each image has been rated on 6 emotion adjectives by 60 Japanese subjects. The database was designed and assembled by Michael Lyons,

<sup>1</sup>Available at <http://www.uk.research.att.com/facedatabase.html>.

<sup>2</sup>Available at [http://www.kasrl.org/jaffe\\_info.html](http://www.kasrl.org/jaffe_info.html)

Miyuki Kamachi, and Jiro Gyoba. See for more details [38].

- Yale<sup>3</sup>: The Yale database contains 165 grayscale images in GIF format of 15 individuals. There are 11 images per subject, one per different facial expression or configuration: center-light, w/glasses, happy, left-light, w/no glasses, normal, right-light, sad, sleepy, surprised, and wink.
- CBCL Face Database<sup>4</sup>: CBCL Face Database is a database of faces and non-faces, that has been extensively used at the center for Center for Biological and Computation Learning at MIT. Here, we choose the training set face, which contains 2,429 faces. Assuming that each has only  $19 \times 19$  pixels.

### B. Compared Algorithms

The following algorithms were compared with our dnsNMF in experiments:

- The *ns*NMF method proposed in [22], i.e., the standard dnsNMF algorithm with a single layer.
- The NMF method proposed in [29].
- The graph regularized NMF (GNMF) [39] which encodes the geometrical information into NMF.
- The Deep Semi-NMF method very recently developed in [27].

For dnsNMF and Deep Semi-NMF, after achieving satisfactory reconstruction error, the toppest layer, i.e.,  $\mathbf{H}_m$ , was used as the feature representation. The clustering performance was measured by two performance indices, the Accuracy (AC) and the Normalized Mutual Information (NMI) (details about these two metrics can be found in [40]).

### C. Visualization of Features

In the aforementioned algorithms, only dnsNMF and Deep Semi-NMF have deep architectures. So the goal of this experiment is compare how dnsNMF and Deep Semi-NMF learn hierarchical parts-based features, respectively. In this experiment, we firstly process the CBCL face data set as did by D.D.Lee and H.S.Seung in [7] and then decompose it by using the dnsNMF and Deep Semi-NMF with three layers. The resulting basis features was visualized as  $19 \times 19$  gray scale images. From Fig.3, it can be seen that dnsNMF gives pixel-level features in the first layer, and edge-based features in the second layer by combining the features generated in the previous layer, and more complex features reflecting entire facial organs in the third layer. As such, a set of parts-based hierarchical features were learnt. Fig.4 shows that counter parts learnt by the Deep Semi-NMF method. Apparently, due to the lack of full nonnegativity constraints, the learning-parts ability was largely damaged, which is one major limitation of Deep Semi-NMF when this parts-based representation plays crucial role in applications. In addition, the corresponding feature representations learned by dnsNMF and Deep Semi-NMF are shown in Fig.5(a) and (b) respectively. It can also be seen

that the data representation learned by dnsNMF is much more sparse than Deep Semi-NMF.

### D. Experiments on Clustering Analysis of Face Images

Similar to [41], for each data set the number of clusters varies from 2 to 10. For simplicity, the facial area of each image was cropped. All of the face images were gray-scaled with the size of  $32 \times 32$  and then were normalized in scale and orientation such that the two eyes are aligned at the same position. Implementation details are as follows:

- 1) For each  $k$ , a total of  $k$  categories from the data set were randomly chosen and shuffled as the collection of samples  $\mathbf{X}$  for clustering.
- 2) The number of features, i.e., the number of rows of  $\mathbf{H}_m$ , was selected to be equal to the number of clusters for clustering analysis for all algorithms (for those without a deep architecture,  $m = 1$ ; otherwise  $m = 2$ ).
- 3) K-means was applied to the extracted features  $\mathbf{H}_m$  for images clustering and repeated 20 times with different initial points and the best result was recorded.

We repeated the above procedure 10 times and recorded the average clustering performance as the final result. All the algorithms had adopted grid search in their parameter spaces to achieve the best accuracy as possible. The dnsNMF and the Deep Semi-NMF were composed of two representation layers in all experiments. To speed up the converge of Deep Semi-NMF, as did in [27], we used an SVD based initialization [42]. Similarly, we used the Non-negative Double Singular Value decomposition (NNDSVD) [43] to speed up dnsNMF.

Fig.6-8 plot the averaged Accuracy and normalized mutual information against different number of clusters on the AT&T ORL, JAFFE and Yale databases, respectively, and TABLE I-III list the detailed clustering accuracy and normalized mutual information. It can be observed that:

- 1) Compared with NMF, *ns*NMF, and GNMF, which are developed to provide part-based representations but without deep architectures, the dnsNMF algorithm always achieved the best clustering performance. This may suggest that a deep architecture does help to improve the performance of NMF.
- 2) Compared to Deep semi-NMF, which has a deep architecture but without parts-based representation guarantee, the dnsNMF achieved improved accuracy. This suggests that, by leveraging the power of both *ns*NMF and deep architectures, the dnsNMF can learn much better features representation for the data than other methods.

### E. Effect of Depth of dnsNMF

In this section, we study how the depth (number of layers) of dnsNMF affects the clustering accuracy. We randomly chose 10 categories from the data set and shuffled the images from these 10 categories for clustering analysis. Then, we applied the dnsNMF method with depth varying from 1 layer to 5 layers to reconstruct  $\mathbf{X}$ . In all the cases, the dimensionality of the toppest layer was fixed to be ten; and the other parameters were chosen using grid search to achieve the best results. The

<sup>3</sup>Available at <http://cvc.yale.edu/projects/yalefaces/yalefaces.html>.

<sup>4</sup>Available at <http://cbcl.mit.edu/cbcl/software-datasets/FaceData2.html>

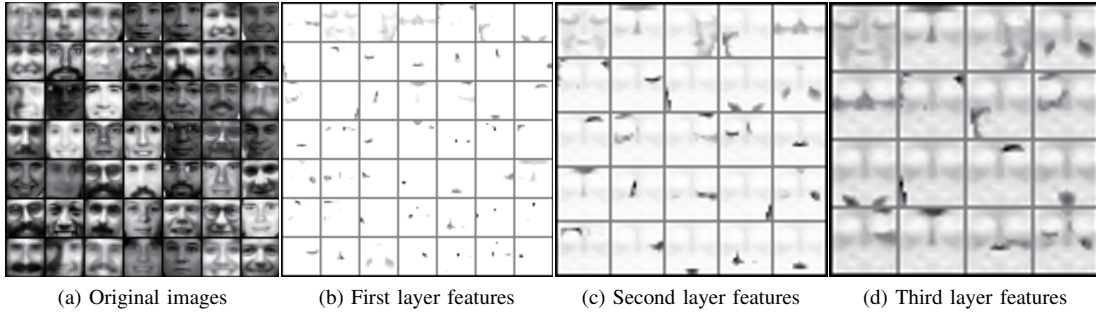


Fig. 3: Features learned by dnsNMF from the CBCL face images database. (a) Original images. (b), (c), (d) show the features created by each layer, which are  $\mathbf{Z}_1$ ,  $\mathbf{Z}_1\mathbf{Z}_2$ , and  $\mathbf{Z}_1\mathbf{Z}_2\mathbf{Z}_3$ , respectively.

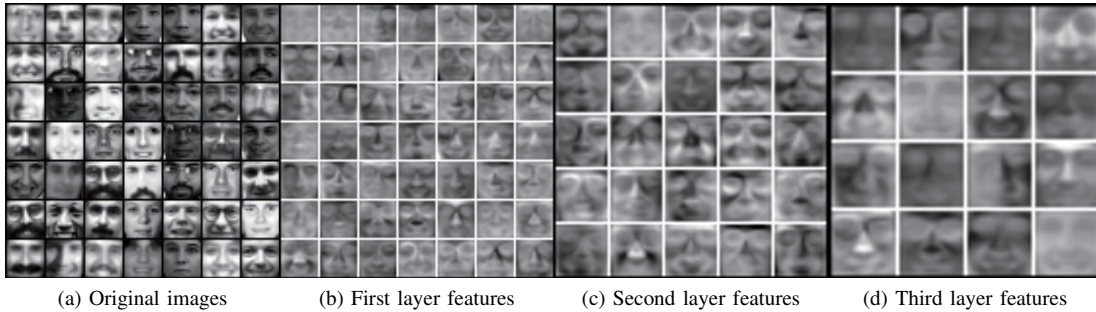


Fig. 4: Features learned by Deep Semi-NMF from the CBCL face images database. (a) Original images. (b), (c), (d) show the features created by each layer, which are  $\mathbf{Z}_1$ ,  $\mathbf{Z}_1\mathbf{Z}_2$ , and  $\mathbf{Z}_1\mathbf{Z}_2\mathbf{Z}_3$ , respectively.

TABLE I: Clustering Performance on AT&T ORL Database

$K$	Accuracy (%)					Normalized Mutual Information (%)				
	NMF	GNMF	<i>ns</i> NMF	Deep Semi-NMF	Deep <i>ns</i> NMF	NMF	GNMF	<i>ns</i> NMF	Deep Semi-NMF	Deep <i>ns</i> NMF
2	85.00	89.00	85.00	86.00	<b>95.00</b>	51.05	59.73	51.05	53.85	<b>76.10</b>
3	80.00	81.00	83.33	81.00	<b>93.33</b>	64.90	70.97	74.03	65.60	<b>84.11</b>
4	69.25	77.15	73.50	72.25	<b>80.00</b>	56.72	65.26	65.10	63.78	<b>69.25</b>
5	74.60	74.00	75.20	77.40	<b>94.60</b>	71.12	72.52	69.38	73.32	<b>88.75</b>
6	67.17	52.50	67.67	70.00	<b>81.67</b>	73.81	61.97	71.73	72.34	<b>83.17</b>
7	69.00	54.43	69.00	72.43	<b>79.43</b>	73.67	55.26	73.27	74.24	<b>77.75</b>
8	74.13	52.13	74.50	77.63	<b>82.13</b>	74.29	63.98	73.20	77.18	<b>82.02</b>
9	66.22	58.67	69.67	71.33	<b>79.78</b>	74.04	63.84	75.65	78.62	<b>80.73</b>
10	70.70	57.70	69.00	77.10	<b>78.50</b>	79.82	67.21	79.71	83.83	<b>87.33</b>
Avg.	72.90	66.29	74.10	76.13	<b>84.94</b>	68.82	64.53	70.35	71.42	<b>81.02</b>

algorithm was tested on AT&T ORL, JAFFE and Yale data sets, respectively, and the results averaged over 10 random runs were plotted in Fig.9. From the figure, the clustering accuracy consistently increases with increasing depth at the early stage and then is nearly invariable with the depth. In these three data sets, it seems that three layers are sufficient to produce satisfactory accuracy. One may question why the performance does keep increasing when the depth further increases. We guess it is because that it is more and more difficult to choose optimal parameters when the number of depth increase gradually. Moreover, the depth efficiency may also rely on the scale of data at hand. Hence, how to choose a proper depth in practical applications deserves further study.

## VI. CONCLUSIONS AND FUTURE WORKS

In this paper, we propose a deep *ns*NMF method which equips *ns*NMF with a deep architecture. The new method is efficient to learn not only part-based but also hierarchical features. We also showed that how dnsNMF can be viewed as a restricted deep autoencoder. Experiments on AT&T ORL, JAFFE and Yale data sets showed that the dnsNMF method can substantially improve clustering accuracy by moderately increasing the depth, demonstrating great potential of dnsNMF as a un-supervising learning method.

Some questions remain to be studied in our future work:

- 1) How to choose a proper depth in practice to achieve a good tradeoff between the accuracy and the efficiency.

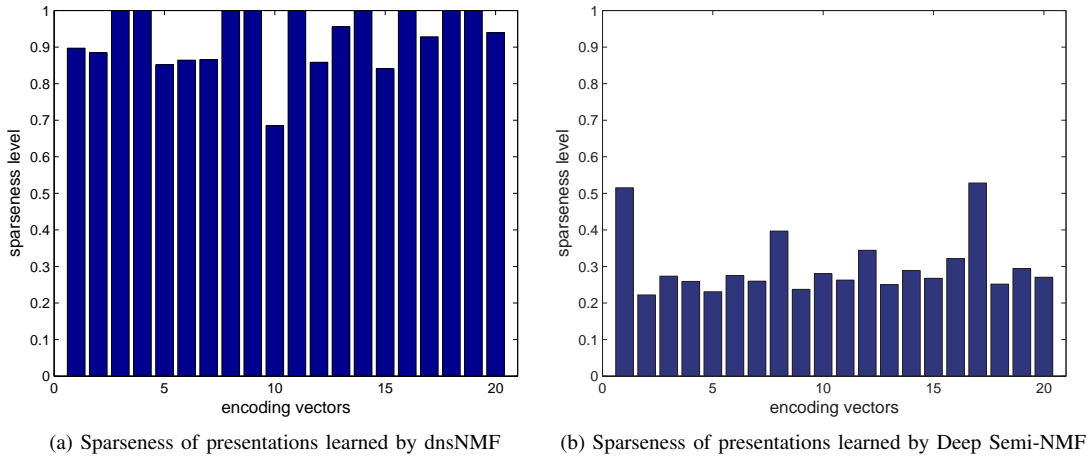


Fig. 5: Illustration of the sparseness level of data representation learned from CBCL data set by dnsNMF (a) and Deep Semi-NMF (b) respectively. Here we illustrate only 20 samples chosen randomly.

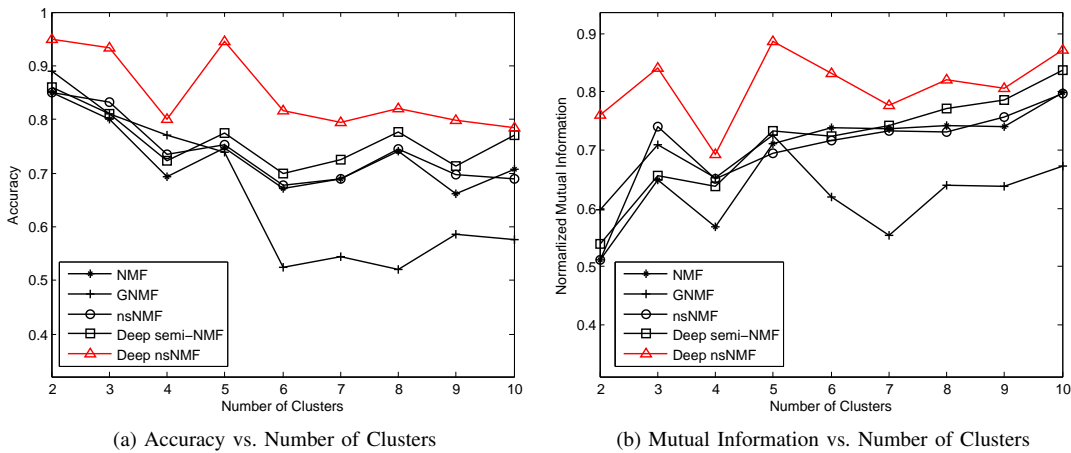


Fig. 6: Clustering performance on the AT&T ORL Database

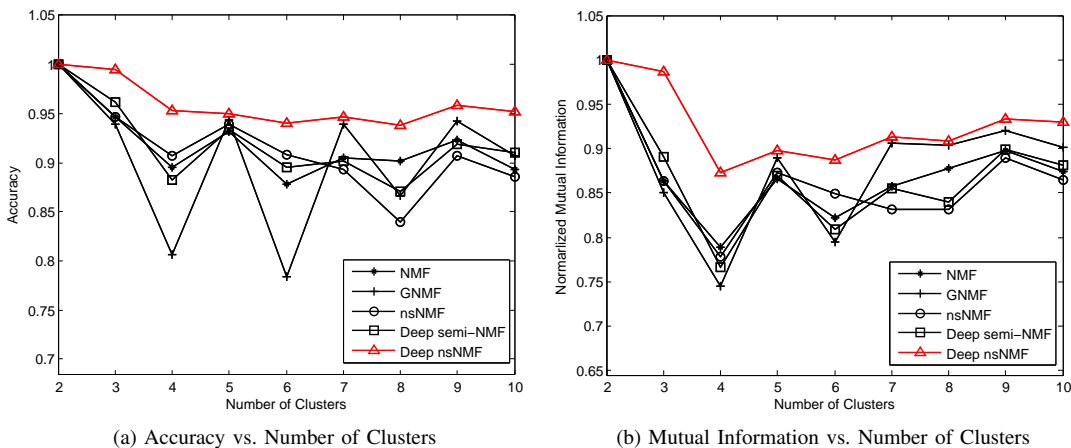


Fig. 7: Clustering performance on the JAFFE Database

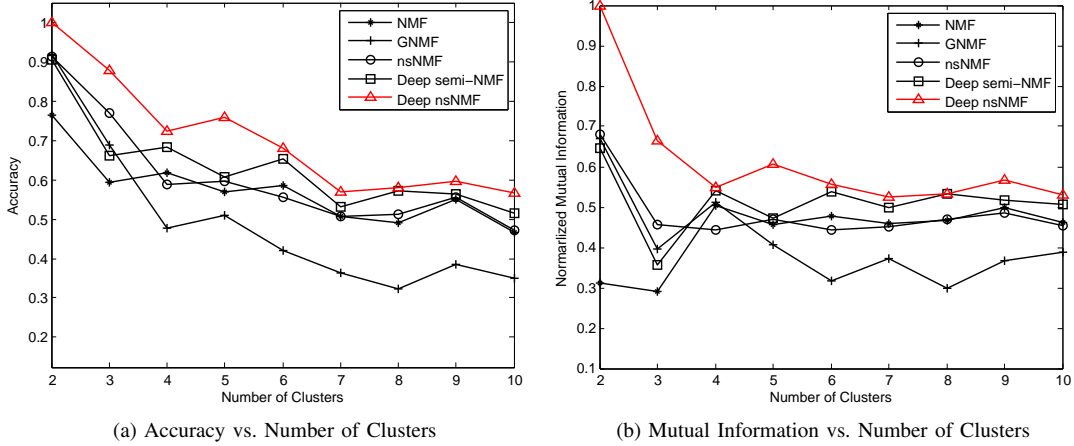


Fig. 8: Clustering performance on the Yale Database

TABLE II: Clustering Performance on JAFFE Database

$K$	Accuracy (%)					Normalized Mutual Information (%)				
	NMF	GNMF	nsNMF	Deep Semi-NMF	Deep nsNMF	NMF	GNMF	nsNMF	Deep Semi-NMF	Deep nsNMF
2	<b>100.00</b>	<b>100.00</b>	<b>100.00</b>	<b>100.00</b>	<b>100.00</b>	<b>100.00</b>	<b>100.00</b>	<b>100.00</b>	<b>100.00</b>	<b>100.00</b>
3	94.68	93.87	94.68	96.13	<b>99.52</b>	86.32	85.01	86.32	89.13	<b>98.71</b>
4	89.54	80.69	90.69	88.28	<b>95.29</b>	78.94	74.51	77.77	76.65	<b>87.35</b>
5	93.14	94.38	93.90	93.43	<b>94.95</b>	86.59	88.90	87.35	86.89	<b>89.76</b>
6	87.85	78.38	90.85	89.54	<b>94.00</b>	82.21	79.52	84.98	80.94	<b>88.76</b>
7	90.54	93.89	89.26	90.20	<b>94.70</b>	85.81	90.58	83.10	85.50	<b>91.29</b>
8	90.12	86.67	83.92	87.08	<b>93.80</b>	87.73	90.42	83.14	83.98	<b>90.87</b>
9	92.36	94.24	90.73	91.88	<b>95.81</b>	89.75	92.05	88.93	89.87	<b>93.36</b>
10	89.34	90.66	88.59	91.08	<b>95.16</b>	87.44	90.15	86.49	88.16	<b>92.96</b>
Avg.	91.95	90.31	91.40	91.96	<b>95.91</b>	87.20	87.90	86.45	86.79	<b>92.56</b>

TABLE III: Clustering Performance on Yale Database

$K$	Accuracy (%)					Normalized Mutual Information (%)				
	NMF	GNMF	nsNMF	Deep Semi-NMF	Deep nsNMF	NMF	GNMF	nsNMF	Deep Semi-NMF	Deep nsNMF
2	76.36	91.82	91.36	90.45	<b>100.00</b>	31.09	66.87	67.93	64.73	<b>100.00</b>
3	59.39	68.79	76.97	66.06	<b>87.88</b>	29.21	39.59	45.75	35.59	<b>66.46</b>
4	61.82	47.73	58.86	68.18	<b>72.27</b>	50.32	51.29	44.24	54.13	<b>54.75</b>
5	56.91	51.09	59.64	60.73	<b>76.00</b>	45.76	40.76	47.06	47.14	<b>60.61</b>
6	58.48	42.12	55.61	65.45	<b>68.03</b>	47.64	31.67	44.46	53.81	<b>55.59</b>
7	50.65	36.36	50.65	53.12	<b>57.01</b>	45.83	37.13	45.19	49.75	<b>52.60</b>
8	49.20	32.39	51.36	57.27	<b>58.07</b>	46.66	29.81	46.88	53.34	<b>53.23</b>
9	55.15	38.59	55.56	56.36	<b>59.60</b>	49.76	36.58	48.66	51.66	<b>56.73</b>
10	46.73	35.09	47.09	51.64	<b>56.64</b>	46.29	38.92	45.27	50.58	<b>52.99</b>
Avg.	57.19	49.33	60.79	63.25	<b>70.61</b>	43.62	41.40	48.38	51.19	<b>61.44</b>

While we believe that the scale of data affect the depth, a further study on this topic is needed.

- 2) Although we have shown that dnsNMF is a restricted deep autoencoder, comparison with deep autoencoder with different activation functions is missing. A comprehensive comparative study could be very interesting.

#### APPENDIX A PROOF OF PROPOSITION 1

**Proof.** According to (19), the gradient of  $E_{Deep}(\mathbf{Z}_i)$

$$\nabla_{\mathbf{Z}_i} E_{deep}(\mathbf{Z}_i) = \mathbf{A}_i^T \mathbf{A}_i \mathbf{Z}_i \mathbf{B}_i \mathbf{B}_i^T - \mathbf{A}_i^T \mathbf{X} \mathbf{B}_i^T. \quad (24)$$

For any two matrices  $\mathbf{Z}_{i1}, \mathbf{Z}_{i2} \in \mathbb{R}^{r_i-1 \times r_i}$ , we have

$$\begin{aligned} & \|\nabla_{\mathbf{Z}_i} E_{deep}(\mathbf{Z}_{i1}) - \nabla_{\mathbf{Z}_i} E_{deep}(\mathbf{Z}_{i2})\|_F^2 \\ &= \|\mathbf{A}_i^T \mathbf{A}_i (\mathbf{Z}_{i1} - \mathbf{Z}_{i2}) \mathbf{B}_i \mathbf{B}_i^T\|_F^2 \\ &= \text{tr}((\mathbf{U}_a \boldsymbol{\Sigma}_a \mathbf{U}_a^T (\mathbf{Z}_{i1} - \mathbf{Z}_{i2}) \mathbf{U}_b \boldsymbol{\Sigma}_b \mathbf{U}_b^T)^T \end{aligned}$$

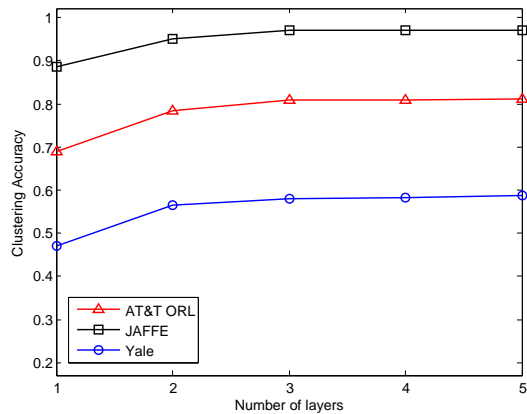


Fig. 9: Effect of depth of the dnsNMF on AT&T ORL, JAFFE and Yale data sets. It illustrates the clustering accuracy of the dnsNMF with depth varying from 1 to 5. It is easy to note that in these three data sets the clustering accuracy consistently increases with increasing depth at the early stage and then is nearly invariable with the added layers.

$$(\mathbf{U}_a \Sigma_a \mathbf{U}_a^T (\mathbf{Z}_{i1} - \mathbf{Z}_{i2}) \mathbf{U}_b \Sigma_b \mathbf{U}_b^T)), \quad (25)$$

where  $\mathbf{U}_a \Sigma_a \mathbf{U}_a^T$  and  $\mathbf{U}_b \Sigma_b \mathbf{U}_b^T$  are the SVD decomposition of  $\mathbf{A}_i^T \mathbf{A}_i$  and  $\mathbf{B}_i \mathbf{B}_i^T$  respectively. and their singular values are  $\{\delta_1, \dots, \delta_{r_i-1}\}$  and  $\{\sigma_1, \dots, \sigma_{r_i}\}$ , which are arranged in descending order. By simple algebraic multiplication, (25) is equivalent to

$$\begin{aligned} & \|\nabla_{\mathbf{Z}_i} E_{deep}(\mathbf{Z}_{i1}) - \nabla_{\mathbf{Z}_i} E_{deep}(\mathbf{Z}_{i2})\|_F^2 \\ &= \text{tr}(\Sigma_a^2 \mathbf{U}_a^T (\mathbf{Z}_{i1} - \mathbf{Z}_{i2}) \mathbf{U}_b \Sigma_b^2 \mathbf{U}_b^T (\mathbf{Z}_{i1} - \mathbf{Z}_{i2})^T \mathbf{U}_a) \\ &\leq \delta_1^2 \text{tr}(\mathbf{U}_a^T (\mathbf{Z}_{i1} - \mathbf{Z}_{i2}) \mathbf{U}_b \Sigma_b^2 \mathbf{U}_b^T (\mathbf{Z}_{i1} - \mathbf{Z}_{i2})^T \mathbf{U}_a) \\ &= \delta_1^2 \text{tr}(\Sigma_b^2 \mathbf{U}_b^T (\mathbf{Z}_{i1} - \mathbf{Z}_{i2})^T (\mathbf{Z}_{i1} - \mathbf{Z}_{i2}) \mathbf{U}_b) \\ &\leq \delta_1^2 \sigma_1^2 \text{tr}(\mathbf{U}_b^T (\mathbf{Z}_{i1} - \mathbf{Z}_{i2})^T (\mathbf{Z}_{i1} - \mathbf{Z}_{i2}) \mathbf{U}_b) \\ &= \delta_1^2 \sigma_1^2 \text{tr}((\mathbf{Z}_{i1} - \mathbf{Z}_{i2})^T (\mathbf{Z}_{i1} - \mathbf{Z}_{i2})) \\ &= \delta_1^2 \sigma_1^2 \|\mathbf{Z}_{i1} - \mathbf{Z}_{i2}\|_F^2. \end{aligned} \quad (26)$$

where  $\delta_1$  and  $\sigma_1$  are the largest singular value of  $\mathbf{A}_i^T \mathbf{A}_i$  and  $\mathbf{B}_i \mathbf{B}_i^T$ , respectively. Note that, the above equations come from the fact that  $\mathbf{U}_a \mathbf{U}_a^T$  and  $\mathbf{U}_b \mathbf{U}_b^T$  are identity matrices. From the (26), we have

$$\begin{aligned} & \|\nabla_{\mathbf{Z}_i} E_{deep}(\mathbf{A}_i, \mathbf{Z}_{i1}, \mathbf{B}_i) - \nabla_{\mathbf{Z}_i} E_{deep}(\mathbf{A}_i, \mathbf{Z}_{i2}, \mathbf{B}_i)\|_F \\ &\leq L_i \|\mathbf{Z}_{i1} - \mathbf{Z}_{i2}\|_F. \end{aligned} \quad (27)$$

Therefore,  $\nabla_{\mathbf{Z}_i} E_{deep}(\mathbf{A}_i, \mathbf{Z}_i, \mathbf{B}_i)$  is Lipschitz continuous and the Lipschitz constant is the product of the largest values of  $\mathbf{A}_i^T \mathbf{A}_i$  and  $\mathbf{B}_i \mathbf{B}_i^T$ , i.e.,  $L_i = \|\mathbf{A}_i^T \mathbf{A}_i\|_2 * \|\mathbf{B}_i \mathbf{B}_i^T\|_2$ . This completes the proof.

## REFERENCES

- [1] P. Paatero and U. Tapper, "Positive matrix factorization: A non-negative factor model with optimal utilization of error estimates of data values," *Environmetrics*, vol. 5, no. 2, pp. 111–126, 1994. [Online]. Available: <http://dx.doi.org/10.1002/env.3170050203>
- [2] J.-P. Brunet, P. Tamayo, T. R. Golub, and J. P. Mesirov, "Metagenes and molecular pattern discovery using matrix factorization," *Proceedings of the National Academy of Sciences*, vol. 101, no. 12, pp. 4164–4169, 2004. [Online]. Available: <http://www.pnas.org/content/101/12/4164.abstract>
- [3] K. Devarajan, "Nonnegative matrix factorization: An analytical and interpretive tool in computational biology," *PLOS Computational Biology*, vol. 4, no. 7, pp. 1–12, 07 2008. [Online]. Available: <https://doi.org/10.1371/journal.pcbi.1000029>
- [4] W. Xu, X. Liu, and Y. Gong, "Document clustering based on non-negative matrix factorization," in *Proceedings of the 26th Annual International ACM SIGIR Conference on Research and Development in Information Retrieval*, ser. SIGIR '03. New York, NY, USA: ACM, 2003, pp. 267–273. [Online]. Available: <http://doi.acm.org/10.1145/860435.860485>
- [5] F. Shahnaz, M. W. Berry, V. Pauca, and R. J. Plemmons, "Document clustering using nonnegative matrix factorization," *Information Processing & Management*, vol. 42, no. 2, pp. 373 – 386, 2006. [Online]. Available: <http://www.sciencedirect.com/science/article/pii/S0306457304001542>
- [6] M. W. Berry and M. Browne, "Email surveillance using non-negative matrix factorization," *Computational & Mathematical Organization Theory*, vol. 11, no. 3, pp. 249–264, Oct 2005.
- [7] D. D. Lee and H. S. Seung, "Learning the parts of objects by non-negative matrix factorization," *Nature*, vol. 401, no. 6755, pp. 788–91, 1999.
- [8] S. Zafeiriou, A. Tefas, I. Buciu, and I. Pitas, "Exploiting discriminant information in nonnegative matrix factorization with application to frontal face verification," *IEEE Transactions on Neural Networks*, vol. 17, no. 3, pp. 683–695, May 2006.
- [9] I. Kotsia, S. Zafeiriou, and I. Pitas, "A novel discriminant non-negative matrix factorization algorithm with applications to facial image characterization problems," *IEEE Transactions on Information Forensics and Security*, vol. 2, no. 3, pp. 588–595, Sept 2007.
- [10] S. Z. Li, X. W. Hou, H. J. Zhang, and Q. S. Cheng, "Learning spatially localized, parts-based representation," in *Proceedings of the 2001 IEEE Computer Society Conference on Computer Vision and Pattern Recognition. CVPR 2001*, vol. 1, 2001, pp. I–207–I–212 vol.1.
- [11] D. Guillamet and J. Vitrià, "Non-negative matrix factorization for face recognition," in *Topics in Artificial Intelligence: 5th Catalanian Conference on AI, CCIA 2002 Castellón, Spain, October 24–25, 2002 Proceedings*, M. T. Escrig, F. Toledo, and E. Golobardes, Eds. Berlin, Heidelberg: Springer Berlin Heidelberg, 2002, pp. 336–344. [Online]. Available: [https://doi.org/10.1007/3-540-36079-4\\_29](https://doi.org/10.1007/3-540-36079-4_29)
- [12] R. Ramanath, W. E. Snyder, and H. Qi, "Eigenviews for object recognition in multispectral imaging systems," in *32nd Applied Imagery Pattern Recognition Workshop, 2003. Proceedings.*, Oct 2003, pp. 33–38.
- [13] F. Weninger and B. Schuller, "Optimization and parallelization of monaural source separation algorithms in the openblissart toolkit," *Journal of Signal Processing Systems*, vol. 69, no. 3, pp. 267–277, Dec 2012. [Online]. Available: <https://doi.org/10.1007/s11265-012-0673-7>
- [14] P. M. Kim and B. Tidor, "Subsystem identification through dimensionality reduction of large-scale gene expression data," *Genome research*, vol. 13, no. 7, pp. 1706–1718, 2003.
- [15] A. Heger and L. Holm, "Sensitive pattern discovery with fuzzy alignments of distantly related proteins," *Bioinformatics*, vol. 19, no. suppl 1, pp. i130–i137, 2003. [Online]. Available: <http://dx.doi.org/10.1093/bioinformatics/btg1017>
- [16] P. Paatero, P. K. Hopke, J. Hoppenstock, and S. I. Eberly, "Advanced factor analysis of spatial distributions of pm2.5 in the eastern united states," *Environmental Science & Technology*, vol. 37, no. 11, pp. 2460–2476, 2003, pMID: 12831032. [Online]. Available: <http://dx.doi.org/10.1021/es0261978>
- [17] P. Smaragdus and J. C. Brown, "Non-negative matrix factorization for polyphonic music transcription," in *2003 IEEE Workshop on Applications of Signal Processing to Audio and Acoustics (IEEE Cat. No.03TH8684)*, Oct 2003, pp. 177–180.
- [18] T. Feng, S. Z. Li, H.-Y. Shum, and H. Zhang, "Local non-negative matrix factorization as a visual representation," in *Proceedings 2nd International Conference on Development and Learning. ICDL 2002*, 2002, pp. 178–183.
- [19] P. O. Hoyer, "Non-negative sparse coding," in *Proceedings of the 12th IEEE Workshop on Neural Networks for Signal Processing*, 2002, pp. 557–565.
- [20] —, "Non-negative matrix factorization with sparseness constraints," *J. Mach. Learn. Res.*, vol. 5, pp. 1457–1469, Dec. 2004. [Online]. Available: <http://dl.acm.org/citation.cfm?id=1005332.1044709>
- [21] W. Liu, N. Zheng, and X. Lu, "Non-negative matrix factorization for visual coding," in *Acoustics, Speech, and Signal Processing, 2003. Proceedings. (ICASSP '03). 2003 IEEE International Conference on*, vol. 3, April 2003, pp. III–293–6 vol.3.
- [22] A. Pascual-Montano, J. M. Carazo, K. Kochi, D. Lehmann, and R. D. Pascual-Marqui, "Nonsmooth nonnegative matrix factorization

- (nsNMF),” *IEEE Transactions on Pattern Analysis and Machine Intelligence*, vol. 28, no. 3, pp. 403–415, March 2006.
- [23] A. Cichocki and R. Zdunek, “Multilayer nonnegative matrix factorization using projected gradient approaches,” *International Journal of Neural Systems*, vol. 17, no. 06, pp. 431–446, 2007, pMID: 18186593. [Online]. Available: <http://www.worldscientific.com/doi/abs/10.1142/S0129065707001275>
- [24] A. Cichocki, R. Zdunek, and S.-i. Amari, “Hierarchical ALS algorithms for nonnegative matrix and 3d tensor factorization,” in *Independent Component Analysis and Signal Separation: 7th International Conference, ICA 2007, London, UK, September 9-12, 2007. Proceedings*, M. E. Davies, C. J. James, S. A. Abdallah, and M. D. Plumbley, Eds. Berlin, Heidelberg: Springer Berlin Heidelberg, 2007, pp. 169–176. [Online]. Available: [https://doi.org/10.1007/978-3-540-74494-8\\_22](https://doi.org/10.1007/978-3-540-74494-8_22)
- [25] A. Cichocki and R. Zdunek, “Multilayer nonnegative matrix factorisation,” *Electronics Letters*, vol. 42, pp. 947–948(1), August 2006. [Online]. Available: [http://digital-library.theiet.org/content/journals/10.1049/el\\_20060983](http://digital-library.theiet.org/content/journals/10.1049/el_20060983)
- [26] H. Zhang, H. Liu, R. Song, and F. Sun, “Nonlinear non-negative matrix factorization using deep learning,” in *2016 International Joint Conference on Neural Networks (IJCNN)*, July 2016, pp. 477–482.
- [27] G. Trigeorgis, K. Bousmalis, S. Zafeiriou, and B. W. Schuller, “A deep matrix factorization method for learning attribute representations,” *IEEE Transactions on Pattern Analysis and Machine Intelligence*, vol. 39, no. 3, pp. 417–429, March 2017.
- [28] Z. Guo and S. Zhang, “Sparse deep nonnegative matrix factorization,” *CoRR*, vol. abs/1707.09316, 2017. [Online]. Available: <http://arxiv.org/abs/1707.09316>
- [29] D. D. Lee and H. S. Seung, “Algorithms for non-negative matrix factorization,” in *Advances in Neural Information Processing Systems 13*, T. K. Leen, T. G. Dietterich, and V. Tresp, Eds. MIT Press, 2001, pp. 556–562. [Online]. Available: <http://papers.nips.cc/paper/1861-algorithms-for-non-negative-matrix-factorization.pdf>
- [30] G. Zhou, A. Cichocki, Q. Zhao, and S. Xie, “Nonnegative matrix and tensor factorizations: An algorithmic perspective,” *IEEE Signal Processing Magazine*, vol. 31, no. 3, pp. 54–65, May 2014.
- [31] Y. Zhang, G. Zhou, Q. Zhao, A. Cichocki, and X. Wang, “Fast nonnegative tensor factorization based on accelerated proximal gradient and low-rank approximation,” *Neurocomputing*, vol. 198, pp. 148 – 154, 2016, advances in Neural Networks, Intelligent Control and Information Processing. [Online]. Available: <http://www.sciencedirect.com/science/article/pii/S0925231216003222>
- [32] N. Guan, D. Tao, Z. Luo, and B. Yuan, “Nnmf: An optimal gradient method for nonnegative matrix factorization,” *IEEE Transactions on Signal Processing*, vol. 60, no. 6, pp. 2882–2898, June 2012.
- [33] D. P. Bertsekas, *Nonlinear Programming*, 2nd ed. Athena Scientific, 1999.
- [34] A. Beck and M. Teboulle, “A fast iterative shrinkage-thresholding algorithm for linear inverse problems,” *SIAM Journal on Imaging Sciences*, vol. 2, no. 1, pp. 183–202, 2009.
- [35] G. Zhou, A. Cichocki, Q. Zhao, and S. Xie, “Efficient nonnegative tucker decompositions: Algorithms and uniqueness,” *IEEE Transactions on Image Processing*, vol. 24, no. 12, pp. 4990–5003, Dec 2015.
- [36] G. W. Cottrell and P. Munro, “Principal components analysis of images via back propagation,” vol. 1001, 1988, pp. 1070–1077. [Online]. Available: <http://dx.doi.org/10.1117/12.969060>
- [37] G. E. Hinton and R. R. Salakhutdinov, “Reducing the dimensionality of data with neural networks,” *Science*, vol. 313, no. 5786, pp. 504–507, 2006. [Online]. Available: <http://science.sciencemag.org/content/313/5786/504>
- [38] M. Lyons, S. Akamatsu, M. Kamachi, and J. Gyoba, “Coding facial expressions with Gabor wavelets,” in *Proceedings Third IEEE International Conference on Automatic Face and Gesture Recognition*, Apr 1998, pp. 200–205.
- [39] D. Cai, X. He, X. Wu, and J. Han, “Non-negative matrix factorization on manifold,” in *2008 Eighth IEEE International Conference on Data Mining*, Dec 2008, pp. 63–72.
- [40] D. Cai, X. He, and J. Han, “Document clustering using locality preserving indexing,” *IEEE Trans. on Knowl. and Data Eng.*, vol. 17, no. 12, pp. 1624–1637, Dec. 2005. [Online]. Available: <http://dx.doi.org/10.1109/TKDE.2005.198>
- [41] H. Liu, Z. Wu, D. Cai, and T. S. Huang, “Constrained nonnegative matrix factorization for image representation,” *IEEE Transactions on Pattern Analysis and Machine Intelligence*, vol. 34, no. 7, pp. 1299–1311, July 2012.
- [42] N. Gillis and A. Kumar, “Exact and heuristic algorithms for semi-nonnegative matrix factorization,” *SIAM Journal on Matrix Analysis and Applications*, vol. 36, no. 4, pp. 1404–1424, 2015. [Online]. Available: <https://doi.org/10.1137/140993272>
- [43] C. Boutsidis and E. Gallopoulos, “SVD based initialization: A head start for nonnegative matrix factorization,” *Pattern Recognition*, vol. 41, no. 4, pp. 1350 – 1362, 2008. [Online]. Available: <http://www.sciencedirect.com/science/article/pii/S0031320307004359>